Role of Counteranions in Acid-Induced Aggregation of Isomeric Tetrapyridylporphyrins in Organic Solvents

Giovanna De Luca, Andrea Romeo, and Luigi Monsù Scolaro*

Dipartimento di Chimica Inorganica, Chimica Analitica e Chimica Fisica, Università di Messina, Salita Sperone 31, 98166 Vill. S. Agata, Messina, Italy

Received: November 8, 2004; In Final Form: February 9, 2005

The effect of adding various kinds of acids HX (X = Cl, Br, I, CF_3COO, CF_3SO_3, TFPB ($(3,5\text{-}(CF_3)_2C_6H_3)_4B$) to isomeric tetra(2-pyridyl)porphyrin, tetra(3-pyridyl)porphyrin, and tetra(4-pyridyl)porphyrin (TpyP(2), TpyP(3), and TpyP(4)) in dichloromethane solution has been investigated through the combined use of UV/vis absorption, fluorescence emission, and resonance light scattering (RLS) techniques. The experimental evidence points to a marked dependence of the protonation and aggregation behavior on the nature of both acids and porphyrins. In general, three different trends can be recognized: (i) formation of a fully protonated species, followed by aggregation; (ii) formation of a tetraprotonated species, which aggregates and, on further addition of acid, disaggregates; and (iii) protonation of the four pyridyl moieties, leading to a tetraprotonated ion pair, in the unique case of the bulky $TFPB^-$ anion. In all cases, the protonated species and the resulting aggregates exhibit spectroscopic features that are markedly influenced by the nature of the counteranions. A model for J-aggregation has been proposed on the basis of an interplay of hydrogen bonding, electrostatic interactions, and dispersive interactions. Kinetic control of the aggregation process allows for a fine-tuning of the spectroscopic properties of the final aggregated species.

Introduction

The formation of porphyrin aggregates in solution through the intermediacy of noncovalent interactions is a well-known phenomenon[1] that affects relevant properties of this class of compounds, including spectroscopic and photophysical features as well as their specific functions. Chemists have challenged themselves with the problem of reproducing a high level of organization in building noncovalent arrays of such molecules in order to mimic biological systems.[2] In this respect, many examples are present in the literature, such as the formation of micrometer-sized porphyrin wheels through solvent evaporation,[3] the self-assembling of chlorophyll analogues in organic solvents,[4] the growth of columnar nanoaggregates through deposition of preformed porphyrin arrays,[5] and the use of microemulsions to get porphyrin nanorods.[6] In aqueous solution, water-soluble porphyrins can be forced to aggregate by properly controlling the pH, ionic strength, and temperature.[7] Electrostatic interactions between charged porphyrins and oppositely charged polymeric matrixes (e.g., nucleic acids, polypeptides,[8] or synthetic polymers[9]) have also been exploited to build assemblies, in which the template can exert a control on the degree of organization of the resulting array. In the absence of a supporting matrix, the formation of highly ordered H- and/or J-aggregates has been reported. These two kinds of aggregates correspond to the limiting cases of *face-to-face* or *edge-to-edge* geometric arrangement for the adjacent stacking monomers. Exciton splitting theory predicts blue-shifted and red-shifted bands with respect to the monomer, for H- and J-aggregates, respectively.[10] In the case of J-aggregates, the so-called J-band is sharp in comparison to that of the monomer and this phenomenon has been explained in terms of motional narrowing, which averages the local inhomogenities.[11] The porphyrin tetrakis(4-sulfonatophenyl)porphyrin ($TPPS_4$) was the first example of a water-soluble species leading to J-aggregates.[12−15] The initial protonation of pyrrole nitrogen atoms to the zwitterionic diacid form has been considered to be responsible for the subsequent growth of linear arrays of stacking monomers, stabilized mainly by the electrostatic interactions between the positively charged inner core and the negative sulfonate groups.

In this framework, diacid porphyrins have attracted a growing interest due to their peculiar structural and spectroscopic features. In particular, in the case of tetraaryl-substituted porphyrins, protonation induces a relevant distortion into the planar geometric arrangement of the parent free base, as revealed in different X-ray crystallographic studies.[16] This class of diacid porphyrins adopts a saddled conformation (D_{2d} symmetry) and the peripheral substituent aryl groups rotate toward the central porphine core, acquiring a more coplanar disposition with respect to the unprotonated species.[17]

Despite the many reports on aggregation phenomena of tetraaryl-substituted porphyrins in aqueous or mixed aqueous−organic phases, very few investigations have been focused strictly on organic solvents.[15,18] During our previous studies on the deposition of porphyrin aggregates through irradiation of dichloromethane or chloroform solutions, we obtained evidence of the presence of large aggregated species formed in solution of tetra(4-pyridyl)porphyrin (TpyP(4)), when the solutions were irradiated for long times.[19] Here we report on the protonation and aggregation behavior of the series of isomeric tetrasubstituted pyridylporphyrins (Figure 1). The investigation has been extended to a series of acids in order to study the effect of the nature of the counteranion on the main spectroscopic features of these systems.

* Corresponding author. Telephone: +39 090 6765711. Fax: +39 090 393756. E-mail: monsu@chem.unime.it.

10.1021/jp0448797 CCC: $30.25
Published on Web 03/17/2005

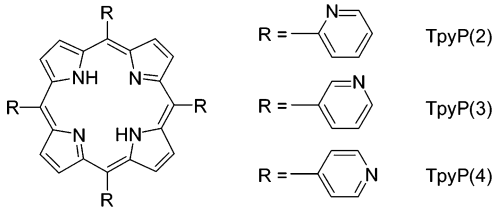

Figure 1. Molecular structures of the investigated porphyrins.

Experimental Section

Chemicals. *meso*-Tetra(4-pyridyl)porphyrin (TpyP(4)) was purchased from Aldrich Chemical Co. and used as received. *meso*-Tetra(3-pyridyl)porphyrin (TpyP(3)) and *meso*-tetra(2-pyridyl)porphyrin (TpyP(2)) were prepared according to literature procedures.[20] Solutions of these porphyrins were prepared in spectrophotometric grade dichloromethane (Sigma). To avoid or minimize dust contamination during light scattering experiments, special care was taken by filtering all the stock solutions through 0.22-μm Millipore filters.

The stock solutions were stored in the dark and used within 1 week from preparation. The range of concentration [$(5-10) \times 10^{-6}$ M] used in our experiments was determined spectrophotometrically using the molar extinction coefficient at the Soret maxima (TpyP(4): 4.54×10^5 M^{-1} cm^{-1}, $\lambda = 416$ nm; TpyP(3): 5.59×10^5 M^{-1} cm^{-1}, $\lambda = 419$ nm; TpyP(2): 3.49×10^5 M^{-1} cm^{-1}, $\lambda = 417$ nm).[20]

All the hydrogen halides, trifluoroacetic acid, and trifluoromethanesulfonic acid were of the highest commercial grade available (Aldrich) and were used as received without further purification. Tetrakis[3,5-bis(trifluoromethyl)phenyl]boric acid (HTFPB) was prepared according to a literature procedure.[21] In the case of hydrogen halides, acidification of the solutions was achieved by injecting acid vapors to a prefixed volume of porphyrin solution having a known concentration (2 mL, [TpyP] $= 3-6$ μM). This injection was performed by using a homemade glass kit connected directly to a reservoir of concentrated acid solution, and the conversion of the porphyrin into the various forms was directly monitored through UV/vis spectroscopy in 1-cm absorption cells. The total amount of added acid was roughly estimated from independent back-titration of dichloromethane solutions of hydrogen halides, using aqueous NaOH. In the case of the other acids, the additions were done by injecting small amounts of neat acid or diluted dichloromethane solutions from a microliter syringe. In all cases, the concentration of the acid stock solutions was high enough to ensure a negligible dilution effect. All the experiments were repeated at least three times to check for reproducibility, and in the case of aggregates precipitation occurs on prolonged standing.

Spectroscopic Methods. UV/vis absorption spectra were measured on a Hewlett-Packard Model HP 8453 diode array spectrophotometer and reported in absorbance units (AU). A UV filter (Hoya glass type UV-34, cutoff 340 nm) was used in all measurements to cut off the UV component of the spectrophotometer lamp, avoiding the formation of HCl by photodecomposition of dichloromethane. Fluorescence emission and excitation spectra and resonance light scattering (RLS) experiments were performed on a Jasco Model FP-750 spectrofluorimeter equipped with a Hamamatsu R928 photomultiplier. For RLS experiments a synchronous scan protocol with a right angle geometry was adopted.[22] Fluorescence and RLS spectra were not corrected for absorption of the samples.

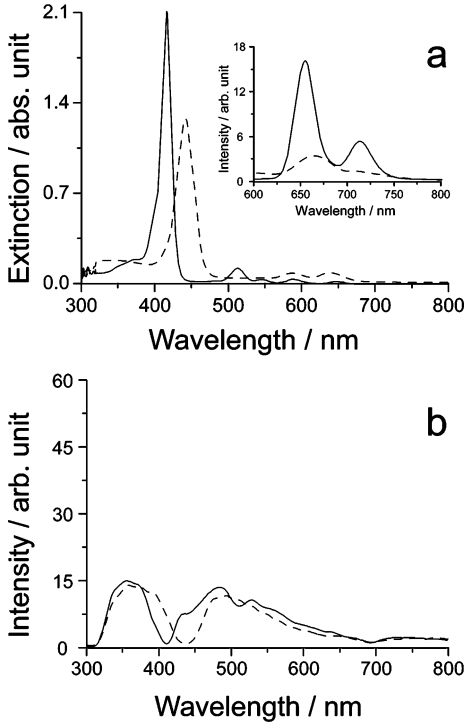

Figure 2. UV/vis (a), RLS (b), and fluorescence emission (inset, $\lambda_{exc} = 420$ nm) spectroscopic changes before (solid line) and after adding CF_3COOH (10 vol %) to a dichloromethane solution of TpyP(4) ([TpyP(4)] $= 4.6$ μM).

Results

Interaction of TpyP(4) with CF_3COOH. According to literature data,[15] addition of large quantities of trifluoroacetic acid (10 vol %) to a dichloromethane solution of TpyP(4) porphyrin produces the expected red shift of the B-band at 441 nm, together with the collapsing of the four Q-bands into two new bands at 587 and 640 nm, respectively (Figure 2a). This behavior is similar to that observed upon coordination of a metal ion into the macrocycle, and is due to the change from a D_{2h} (the free base) to a D_{2d} symmetry (the diacid species) of the porphine core. Fluorescence spectra are also deeply affected by protonation. The typical two-band emission of the free base, Q(0,0) and Q(0,1), undergoes a red shift and broadening (inset of Figure 2a). The monomeric nature of the protonated species has been confirmed by RLS experiments, which show that both the free base and the protonated form exhibit rather weak light scattering profiles with wells due to photon absorption at the wavelengths of the corresponding B-bands (Figure 2b). All this experimental evidence confirms the previously reported assignment of this species to the fully protonated $H_6TpyP(4)^{6+}$.[15]

A rather different behavior is evident when CF_3COOH is added in small subsequent amounts. On increasing the acid concentration, the UV/vis spectra show a gradual conversion to a new species with a Soret band at 431 nm and four Q-bands, all red shifted with respect to the unprotonated species (Figure 3a). When more acid is added, a further bathochromic shift is observed in the Soret band, which moves to 444 nm, while the Q-band region presents three different features (Figure 3b). Additional acid causes the conversion of this latter species into a final one, having a Soret band at 441 nm and a set of three Q-bands at 546, 587, and 640 nm (Figure 3c), whose spectroscopic features are almost coincident with those reported in the literature under strongly acidic conditions. It is worth noting the substantial hypochromicity of the spectra on passing from the free base TpyP(4) to the two new subsequent species and

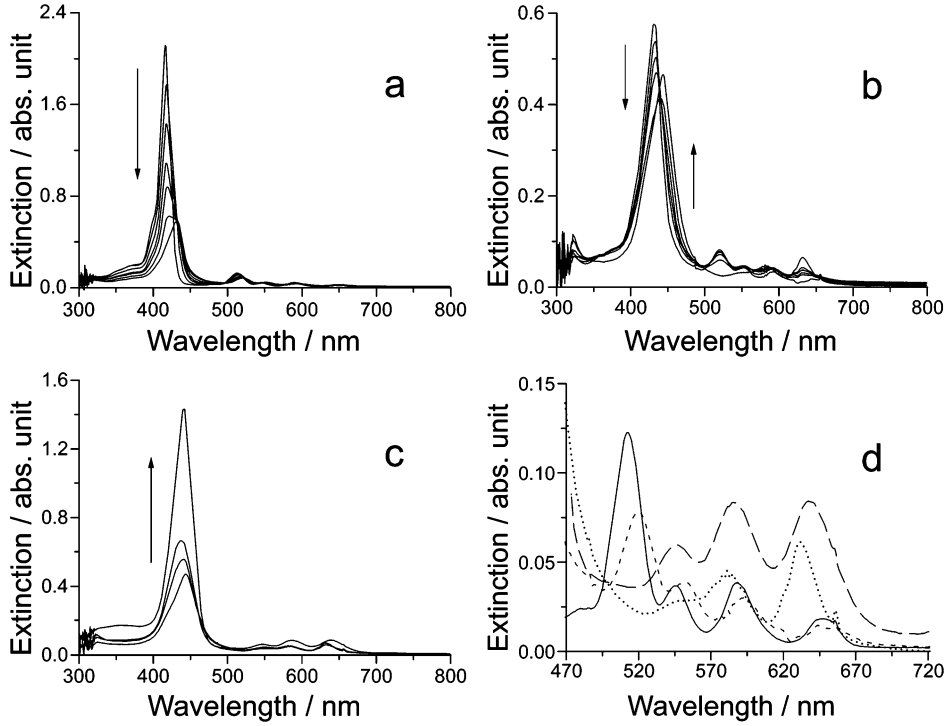

Figure 3. UV/vis spectral changes following stepwise addition of CF_3COOH to dichloromethane solution of TpyP(4) ([TpyP(4)] = 4.6 μM). (a−c) Gradual formation of various species; arrows mark the increase of acid concentration (a, up to 200 μM; b, up to 900 μM; c, up to 80 mM). (d) Expansion of the Q-band region: TpyP(4) (solid line), $H_4TpyP(4)^{4+}{}_{agg}$ (short dashed line), $H_5TpyP(4)^{5+}{}_{agg}$ (dotted line), and $H_6TpyP(4)^{6+}$ (long dashed line).

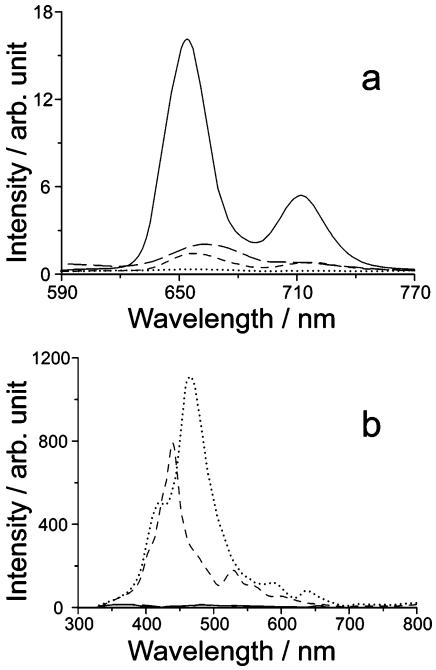

Figure 4. Fluorescence emission spectra (a) and RLS spectra (b) for various species obtained by stepwise addition of CF_3COOH to dichloromethane solution of TpyP(4) ([TpyP(4)] = 4.6 μM): TpyP(4) (solid line), $H_4TpyP(4)^{4+}{}_{agg}$ (short dashed line), $H_5TpyP(4)^{5+}{}_{agg}$ (dotted line), and $H_6TpyP(4)^{6+}$ (long dashed line).

the almost complete recovery of the intensity with the final species. Fluorescence emission spectra recorded during the experiments show a consistent quenching of the emission with respect to the parent porphyrin (Figure 4a). The first species exhibits a red shift of 3 nm in the emission maxima. The emission of the second species is almost completely quenched, while the spectra corresponding to the final species are higher than the first one and further red shifted. RLS experiments show the presence of intense features, with maxima at 439 and 465 nm, respectively, in samples containing the first and second species (Figure 4b). The final species only shows a well in the very weak RLS profile, due to photon absorption at 441 nm. All the experimental evidence allows us to assign the first species to the porphyrin having the four pyridyl moieties protonated. The protonation of the pyrrole nitrogen atoms can be ruled out on the basis of the presence of four Q-bands. This species is slightly aggregated, as confirmed by the occurrence of a fairly strong peak in the RLS spectra, and it is still emissive ($H_4TpyP(4)^{4+}{}_{agg}$). The second species evidences a completely different pattern for the Q-bands, with respect to $H_4TpyP(4)^{4+}{}_{agg}$ and to the final fully protonated form. The fluorescence emission is completely quenched, in agreement with its strongly aggregated form, which is further proved by the occurrence of a strong RLS peak close to the absorption. These spectral features can be tentatively assigned to a fully aggregated porphyrin, having four protonated pyridyl moieties and being monoprotonated at the inner nitrogen core ($H_5TpyP(4)^{5+}{}_{agg}$). The final species is virtually coincident with that obtained under strongly acidic conditions ($H_6TpyP(4)^{6+}$).

Interaction of TpyP Isomers with HCl. Upon addition of hydrochloric acid, TpyP porphyrin isomers exhibit different patterns of behavior, which are again different with respect to the previously described example. In the case of TpyP(4), Figure 5 displays the UV/vis spectral changes on increasing the HCl concentration. The B- and Q-bands of the free base undergo gradual hypochromicity and bathochromic shift. No distinct isosbestic points can be detected, and the final solution evidences a large Rayleigh scattering component. The initial fluorescence emission is consistently reduced at an intermediate stage of the process, and the spectra show a slight red shift. The corresponding RLS spectra exhibit a large component that is strongly modulated by absorbance of the sample. The region of the

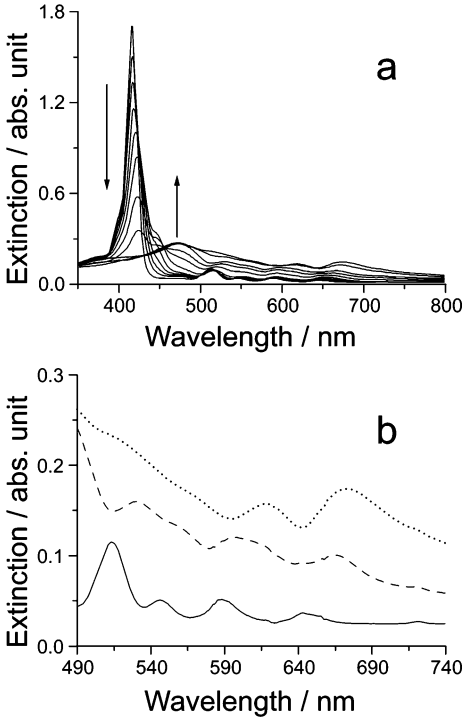

Figure 5. UV/vis spectral changes following stepwise addition of HCl to dichloromethane solution of TpyP(4) ([TpyP(4)] = 3.7 μM, final HCl concentration ~1 mM). (b) Expansion of the Q-band region: TpyP(4) (solid line), $H_4TpyP(4)^{4+}{}_{agg}$ (dashed line), and $H_6TpyP(4)^{6+}{}_{agg}$ (dotted line).

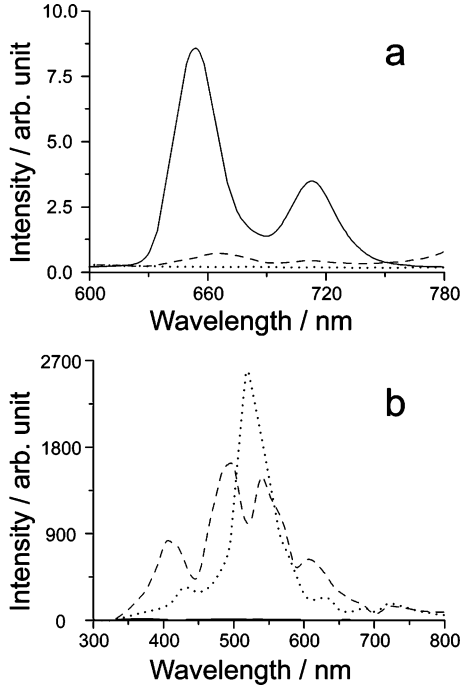

Figure 6. Fluorescence emission spectra (a) and RLS spectra (b) for various species obtained by adding HCl to dichloromethane solution of TpyP(4) ([TpyP(4)] = 3.7 μM): TpyP(4) (solid line), $H_4TpyP(4)^{4+}{}_{agg}$ (dashed line), and $H_6TpyP(4)^{6+}{}_{agg}$ (dotted line).

Q-bands displays a four-band pattern (Figure 5b), which suggests the presence of a tetraprotonated species at the peripheral pyridyl groups ($H_4TpyP(4)^{4+}{}_{agg}$). The final species is characterized by a broad extinction spectrum, with non-null extinction all over the visible range. The main peak is located at 470 nm and is accompanied by two distinguishable Q-bands, which point to a fully protonated species ($H_6TpyP(4)^{6+}{}_{agg}$). The occurrence of large aggregates is proved by an almost complete quenching of fluorescence emission and by the presence of a very intense and defined peak in the RLS spectra (Figure 6).

When hydrochloric acid is added to a solution of TpyP(2), the UV/vis spectra evidence the formation of two well distinct species, through a series of spectral changes displaying defined isosbestic points (Figure 7). In an initial stage, the Soret band of TpyP(2) undergoes a bathochromic shift, while three new Q-bands can be easily detectable at 558, 605, and 657 nm, respectively. The corresponding fluorescence emission spectra exhibit a red shift of the two maxima, together with reduction of the intensity (Figure 8). All this evidence, together with a low RLS profile, allows for an assignment of these spectral features to the unaggregated fully protonated porphyrin ($H_6TpyP(2)^{6+}$). Further addition of HCl causes the gradual conversion of this latter species into a final one, which is characterized by a much broader, red-shifted and hypochromic Soret band. According to the presence of extended aggregates ($H_6TpyP(2)^{6+}{}_{agg}$), the fluorescence emission is completely quenched and the RLS spectra show an very intense feature located at 512 nm. A strictly similar pattern of behavior is exhibited by TpyP(3) porphyrin, upon treatment with HCl (data not shown).

Interaction with a Series of HX. The previous experimental data have clearly pointed out a strong dependence of the spectroscopic properties on the nature of the counterions. Tables 1−3 collect the main spectroscopic features (UV/vis absorption, fluorescence emission, and RLS) of the species clearly detected for the three isomeric porphyrins in the presence of a variety of acids (HX; X = Cl, Br, I, CF_3COO, CF_3SO_3, TFPB). The assignment to the various protonated forms has been performed according to the number and pattern of the Q-bands. The aggregation state has been attributed on the basis of the presence of intense RLS peaks.

An inspection of these data shows that in the case of the halogen anions a trend very similar to that already reported for TPP diacids can be observed.[17] The B-band, at least for the final aggregated species, has the lowest energy for the bromide and the highest for the iodide. In the case of these latter anions, the fluorescence emission is quenched, since low-lying halide to porphyrin charge transfer (HPCT) excited states offer additional decay paths that further enhance the radiationless decay.[17]

It is interesting to note the behavior of the bulky tetrakis-(3,5-bis(trifluoromethyl)phenyl)borate anion (TFPB). This species has been exploited as a lypophilic noncoordinating anion mainly in preparing organometallic complex cations.[23] Addition of this acid to a solution of TpyP(4) (the pattern of behavior of the other two isomeric porphyrins being essentially the same) leads to a bathochromic shift of the B- and Q-bands (Figure 9). In particular, the Q-bands do not change in number, indicating protonation of the peripheral pyridyl groups, without involving the central core. The fluorescence emission spectra display a bathochromic shift of the two maxima, with a partial reduction of the intensity. According to the monomeric nature of this species, the RLS profile evidences a low intensity with wells corresponding to the absorption maxima (Figure 10).

Discussion

According to literature data,[15] the experimental evidence on the protonation of TpyP(4) porphyrin with CF_3COOH (Figures 2−4) clearly points out that the existence of a fully protonated and monomeric form of this compound is confined in strongly acidic media. A stepwise increase of acid concentration allows

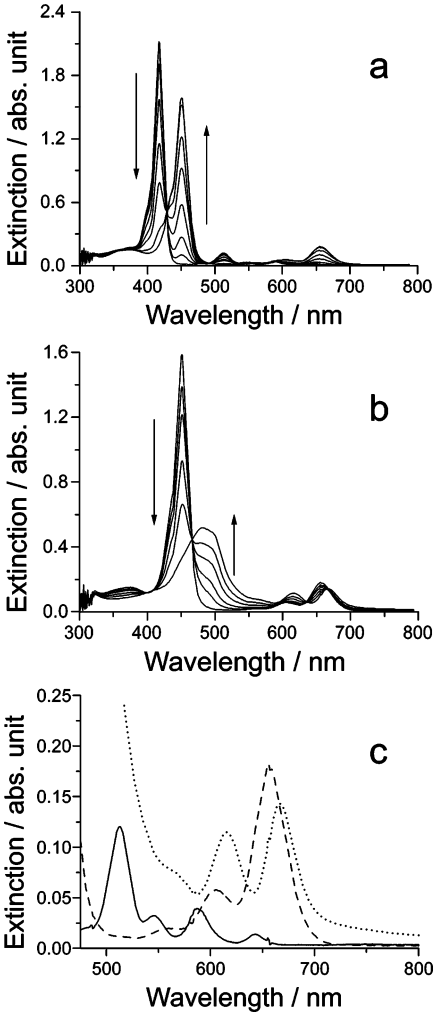

Figure 7. UV/vis spectral changes following stepwise addition of HCl to dichloromethane solution of TpyP(2) ([TpyP(2)] = 6.0 μM). (a, b) Gradual formation of various species; arrows mark the increase of acid concentration (a, up to ~500 μM; b, up to ~2 mM). (c) Expansion of the Q-band region: TpyP(2) (solid line), $H_6TpyP(2)^{6+}$ (dashed line), and $H_6TpyP(2)^{6+}{}_{agg}$ (dotted line).

for the detection of various intermediate species, exhibiting different degrees of protonation and aggregation.

All the experimental data collected in Tables 1−3 evidence a variety of patterns of behavior, which depend on the specific porphyrin isomer and on the counteranion (Figure 11). Three general behaviors can be easily envisaged: (i) The formation of a four-protonated ion pair is the first step, followed by further addition of two protons in the inner nitrogen core and subsequent aggregation (TpyP(2)/Cl^-, Br^-, $CF_3SO_3^-$; TpyP(3)/Cl^-, -Br^-, -I^-). (ii) After the initial four-protonated ion pair is generated, aggregation occurs; on increasing the acid concentration, a fully hexaprotonated and monomeric species is formed (TpyP(3)/$CF_3SO_3^-$; TpyP(4)/CF_3COO^-, -$CF_3SO_3^-$). (iii) In the case of $TFPB^-$ anion, a four-protonated ion pair is the unique species in solution, as a result of the steric hindrance of this particular anion. A variant to route i is evident with the systems TpyP(4)/Cl^-, -Br^-, -I^-, in which a smooth formation of protonated species leads to the final $\{(H_6TpyP^{6+})(X^-)_6\}_{agg}$. In case ii, when the TpyP(4)/CF_3COOH system is considered, the formation of a pentaprotonated ion pair $\{(H_5TpyP(4)^{5+})(CF_3COO^-)_5\}$ (monoacid porphyrin) has been invoked on the basis of the pattern exhibited by the Q-bands. Indeed, very few literature reports deal with a clear identification of such species for tetraarylporphyrins. Early studies by Aronoff[24] on protonation of porphyrins in dioxane as solvent and using perchloric acid indicated the presence of a monoprotonated species for tetraphenylporphyrin, having different optical features with respect to the free base and the diacid form. The corresponding UV/vis spectra show a pattern with three Q-bands in which the two at lower energies display comparable extinction coefficients. Later reports on TpyP(4) in aqueous solutions described the formation of monoacid species, attributing a three Q-band spectrum to this intermediate.[25]

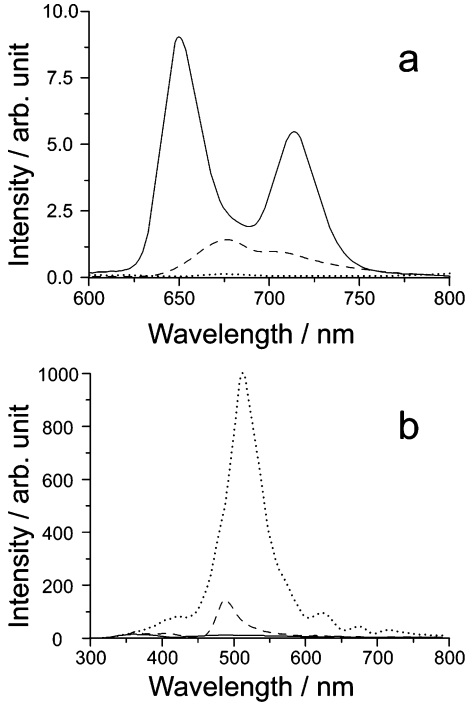

Figure 8. Fluorescence emission spectra (a) and RLS spectra (b) for various species obtained by adding HCl to dichloromethane solution of TpyP(2) ([TpyP(2)] = 6.0 μM): TpyP(2) (solid line), $H_6TpyP(2)^{6+}$ (dashed line), and $H_6TpyP(2)^{6+}{}_{agg}$ (dotted line).

A few systems exhibit trends that cannot be classified into the previous series (e.g., TpyP(2) and TpyP(3) with CF_3COO^-, and TpyP(2) with I^-). In these cases, species having different degrees of protonation are formed, but no aggregation is evident, even fostering acid concentration.

It is worth noting that, except for very few cases during the initial stage of acid addition, isosbestic points are not completely held, suggesting the stepwise formation of gradually protonated species at the peripheral pyridyl substituent groups.

Effect of Counterions and Porphyrins. An inspection of the data relative to a specific isomeric porphyrin clearly shows that the main spectroscopic features are strongly influenced by the nature of the counterion. Indeed, the simple tetraphenylporphyrin (TPP) in dichloromethane displays optical properties that are strongly modulated by the anions. In the case of the halides, the ion pairs $\{(H_6TpyP^{6+})(X^-)_6\}$ evidence a trend in the wavelength position of the B-band, which parallels that exhibited by the corresponding $\{(H_2TPP^{2+})(X^-)_2\}$ ($I^- < Cl^- < Br^-$).[17] The oxygen donor anions (CF_3COO^- and $CF_3SO_3^-$) display B-bands located at slightly higher energies.

An analysis of $\{(H_2TPP^{2+})(X^-)_2\}$ (X = F, Cl, Br, I) diacid species has been recently performed through DFT and TDDFT calculations.[17] A dissection of the energy contribution has shown that, apart from electrostatics, covalent interactions are a relevant component in the total energy for the hydrogen bonding between the protonated N−H groups and the counteranions. In addition

TABLE 1: UV/Vis Absorption, Emission, and RLS Features of TpyP(4) Porphyrin Derived Species in the Presence of Various HX in Dichloromethane at 298 K

X	species	B-band (λ/nm)	Q-bands (λ/nm)				emission maxima (λ/nm)		RLS
	TpyP(4)	416	513	546	589	646	653	713	
Cl^-	$H_4TpyP(4)^{4+}_{agg}$	450	530	559	597	658	666	711	492
Cl^-	$H_6TpyP(4)^{6+}_{agg}$	470			619	674			515
Br^-	$H_4TpyP(4)^{4+}_{agg}$	448	527	559	592	667	676	712	476
Br^-	$H_6TpyP(4)^{6+}_{agg}$	492			619	671			517
I^-	$H_4TpyP(4)^{4+}_{agg}$	440	528	561	593	670			468
I^-	$H_6TpyP(4)^{6+}_{agg}$	470			626	688			493
CF_3COO^-	$H_4TpyP(4)^{4+}_{agg}$	431	520	553	593	649	657	716	439
CF_3COO^-	$H_5TpyP(4)^{5+}_{agg}$	444		550	582	632			465
CF_3COO^-	$H_6TpyP(4)^{6+}$	441		546	587	640	665	707	
$CF_3SO_3^-$	$H_4TpyP(4)^{4+}_{agg}$	461		546	591	639	674	712	479
$CF_3SO_3^-$	$H_6TpyP(4)^{6+}$	451		545	591	643	669	709	
$TFPB^-$	$H_4TpyP(4)^{4+}$	433	522	561	597	658	666	723	

TABLE 2: UV/Vis Absorption, Emission, and RLS Features of TpyP(3) Porphyrin Derived Species in the Presence of Various HX in Dichloromethane at 298 K

X	species	B-band (λ/nm)	Q-bands (λ/nm)				emission maxima (λ/nm)		RLS
	TpyP(3)	419	515	550	590	645	650	715	
Cl^-	$H_6TpyP(3)^{6+}$	447			605	656	668	712	
Cl^-	$H_6TpyP(3)^{6+}_{agg}$	461		556	604	652	667		488
Br^-	$H_6TpyP(3)^{6+}$	452			604	655	669	714	
Br^-	$H_6TpyP(3)^{6+}_{agg}$	484		557	604	652	663		487
I^-	$H_6TpyP(3)^{6+}$	442			617	673			
I^-	$H_6TpyP(3)^{6+}_{agg}$	449			613	663			480
CF_3COO^-	$H_6TpyP(3)^{6+}$	439		547	588	638	664	708	
$CF_3SO_3^-$	$H_4TpyP(3)^{4+}_{agg}$	442	519	550	588	635			459
$CF_3SO_3^-$	$H_6TpyP(3)^{6+}$	436		540	583	634	656	709	
$TFPB^-$	$H_4TpyP(3)^{4+}$	428	515	550	593	644	651	718	

TABLE 3: UV/Vis Absorption, Emission, and RLS Features of TpyP(2) Porphyrin Derived Species in the Presence of Various HX in Dichloromethane at 298 K

X	species	B-band (λ/nm)	Q-bands (λ/nm)				emission maxima (λ/nm)		RLS
	TpyP(2)	417	513	546	588	643	649	713	
Cl^-	$H_6TpyP(2)^{6+}$	451		558	605	657	677	708	487
Cl^-	$H_6TpyP(2)^{6+}_{agg}$	487		568	615	667			512
Br^-	$H_6TpyP(2)^{6+}$	457		557	608	659	678	707	494
Br^-	$H_6TpyP(2)^{6+}_{agg}$	484		566	616	666			505
I^-	$H_6TpyP(2)^{6+}$	433			618	666	657	712	
I^-	$H_6TpyP(2)^{6+}_{agg}$	486				630			a
CF_3COO^-	$H_4TpyP(2)^{4+}$	442	517	550	594	647	673	709	
CF_3COO^-	$H_6TpyP(2)^{6+}$	450		552	594	644	666	713	
$CF_3SO_3^-$	$H_4TpyP(2)^{4+}$	439	524	550	594	653	668	723	
$CF_3SO_3^-$	$H_6TpyP(2)^{6+}$	452		523	598	651	663	730	
$CF_3SO_3^-$	$H_6TpyP(2)^{6+}_{agg}$	480			597	647	652	710	482
$TFPB^-$	$H_4TpyP(2)^{4+}$	428	520	557	593	649	663	719	

[a] On the basis of the pattern of behavior very similar to the other halides, this feature has been tentatively attributed to the aggregated species. The absence of any detectable RLS signal could be explained by a smaller size of the resulting clusters (less than 25 porphyrins, ref 26).

to porphyrin core distortion and phenyl group twisting, a strong interaction between the π-systems of the central porphine and of the substituent groups occurs, leading to a consistent splitting of the occupied Gouterman orbitals. The decrease of the gap between a_{2u} and e_g*, together with the lifting of the a_{2u}/a_{1u} degeneracy, is the main explanation for the observed bathochromic shift of both the B- and Q-bands. An important finding of this theoretical analysis is that the set of highest occupied molecular orbitals (apart from the Gouterman orbitals) is constituted by the halide lone pair orbitals, explaining the observed dependence of both the UV/vis transitions and fluorescence emission on the nature of the halide.

Fixing the type of counteranion, the differing spatial disposition of the pyridine nitrogen atom on the peripheral group has an impact on the specific behavior of the protonated porphyrins. We will discuss this effect on considering the behavior of the three isomers with HCl. TpyP(4) shows a gradual change in the extinction spectra upon addition of this acid, without evidencing a clear distinction between the various species (Figure 5). In contrast, TpyP(2) and TpyP(3) exhibit well distinct isosbestic points during the stepwise conversion. Different from TpyP(4), both these porphyrins evidence a marked coexistence between the initial free base and the unaggregated hexaprotonated $\{(H_6TpyP^{6+})(Cl^-)_6\}$ ion pair. To the best of our knowledge, there are no reports in the literature on the pK_a values for the protonation of the peripheral pyridyl moieties, while the values for the first protonation step of the inner nitrogen atoms have been measured in dichloromethane (TpyP(4), 1.8; TpyP(3), 2.1; TpyP(2), 1.2).[20] Usually, the pK_a of the central pyrrolic nitrogen atoms can be regarded as a good probe for the effect of the substituent groups on the porphine core. In aqueous solution, N-methylation at the pyridyl peripheral groups makes the inner core more acidic (e.g., $\Delta pK_a = -2.1$ for TMpyP(2) vs TpyP(2)). In a solvent having a low dielectric constant, i.e.,

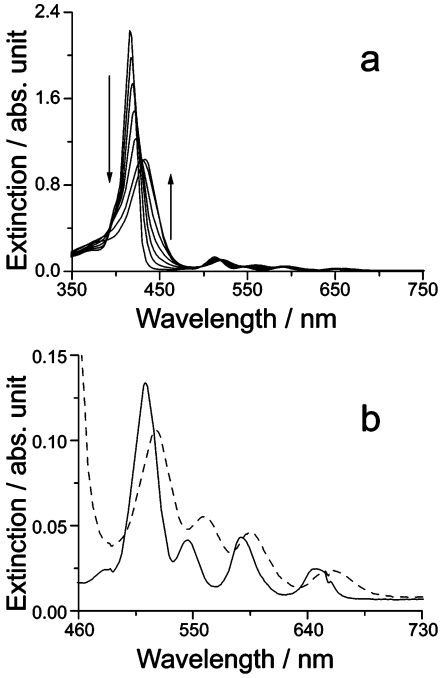

Figure 9. UV/vis spectral changes (a) following stepwise addition of HTFPB to dichloromethane solution of TpyP(4) ([TpyP(4)] = 4.9 μM, final HTFPB concentration 250 μM). (b) Expansion of the Q-band region: TpyP(4) (solid line) and $H_4TpyP(4)^{4+}$ (dashed line).

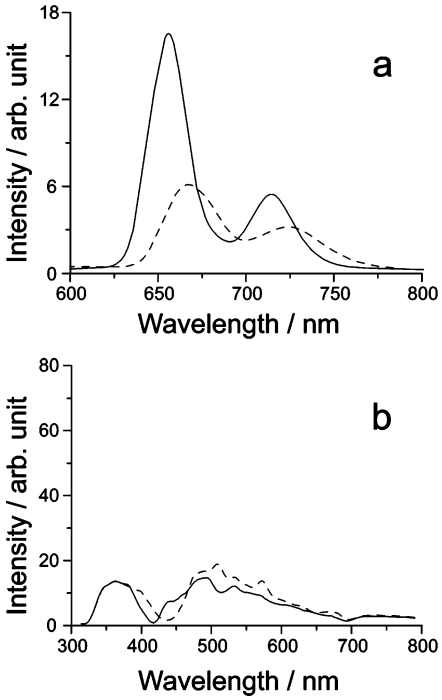

Figure 10. Fluorescence emission spectra (a) and RLS spectra (b) for species obtained by adding HTFPB to dichloromethane solution of TpyP(4) ([TpyP(4)] = 4.9 μM): TpyP(4) (solid line) and $H_4TpyP(4)^{4+}$ (dashed line).

dichloromethane, ion pairing should be favored and our experimental findings suggest that initial protonation at the periphery does not seem to play an important role in reducing the subsequent protonation of the central core.

The behavior of the bulky $TFPB^-$ anion is rather interesting. This species has been widely used in organometallic chemistry and especially in catalysis, to reduce the binding of the counteranion to extremely reactive or coordinatively unsaturated cationic complex ions.[23] In our hands, this anion has invariably led to the formation of unaggregated tetraprotonated $\{(H_4TpyP^{4+})(TFPB^-)_4\}$ ion pairs. The four sterically demanding anions close to the peripherally protonated porphyrin hinder the further approach of a fifth $TFPB^-$ anion, blocking also the proton transfer. The absence of protonation at the central porphine core supports the important role played by hydrogen bonding in stabilizing the mono- and diacid species in apolar solvents.

Aggregation. The counteranion also affects the nature and extent of aggregation. The smaller and spherical halide anions in all the investigated porphyrins (with the exception of TpyP(2) and iodide) eventually lead to the formation of fully protonated aggregated species, as probed by the presence of bathochromically shifted, hypochromic, and broader extinction bands. The large size of these aggregates is confirmed by very intense RLS peaks located at the red edge portion of the absorption features. RLS effect arises from an enhancement of the scattered light intensity in close proximity to an absorption band for strongly aggregated chromophores.[22,26]

The large red shift of the aggregate B-bands ($\Delta\lambda = +30-40$ nm) is consistent with an edge-to-edge (J-type) geometric arrangement of the porphyrins in the growing structures. J-aggregates have been so far reported for the water-soluble $TPPS_4$[12−15] and for a few other cases.[27] In analogy with the proposed structural arrangement of the zwitterionic $TPPS_4$ in J-aggregates, we are inclined to think that halide anions can stabilize the present aggregates by participating in a network of hydrogen bonds, which involve the protonated pyrrole nitrogen atoms of the macrocycle and the protonated pyridyl moieties. Apart from this specific interaction, electrostatic ion pairing and π-stacking interactions should play an important role in stabilizing the overall structure. Figure 12 reports the proposed model in the case of TpyP(4) isomer. Even if the different positions of the nitrogen atom on the pyridyl group can affect the final structure, the available data point to an efficient stabilization, probably related to the facility for the spherically shaped anions to accommodate inside the network. In the case of TpyP(2) and TpyP(3) the occurrence of several different rotamers also appears to be probable. Interestingly, the RLS profile for these kinds of aggregates is rather sharp and very similar to that already reported for $TPPS_4$ J-aggregates,[14] indicating good quality of the optical resonance. A different kind of profile is exhibited by the $\{(H_4TpyP(4)^{4+})(X^-)_4\}_{agg}$ species (X = Cl, Br, I), in which the RLS envelope is not sharp and it is strongly modulated by absorption of the sample. This observation can be explained in terms of the different electronic couplings between the tetra- and hexaprotonated species, due to the different geometric features and steric demands of the two types of porphyrins. It is known that, taking into account the distortion of the porphine plane and the rotation of the aryl groups,[17] hexaprotonated porphyrins (diacids) exhibit a more planar structure with respect to the parent free base or, in the present case, to the tetraprotonated species. Simple calculations on molecular models reveal that the mean width of a fully protonated species is less than 4 Å, while this size increases to 4.5 Å for a free base or a peripherally protonated species. The looser structure of $\{(H_4TpyP(4)^{4+})(X^-)_4\}_{agg}$ versus $\{(H_6TpyP(4)^{6+})(X^-)_6\}_{agg}$ is still supported by the reduced but not completely quenched fluorescence emission of the former species in comparison with the latter ones.

In the case of CF_3COO^- anion interacting with TpyP(4), after the buildup of tetraprotonated ion pairs, which start to aggregate, the electronic spectra in the Q-band region seem to suggest the formation of aggregated monoacid species (at the core). Dif-

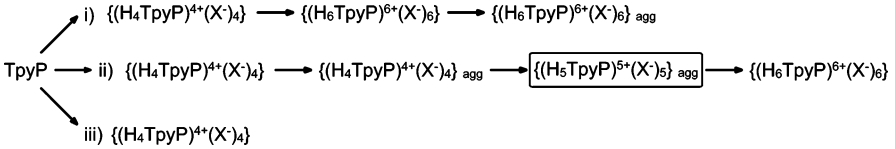

Figure 11. Sequences of observed pattern of behavior for protonation/aggregation of isomeric porphyrins TpyP with various HX in dichloromethane. The boxed species has been observed for TpyP(4)/CF_3COOH system. For the sake of simplicity, explicit addition of HX in each step has been omitted.

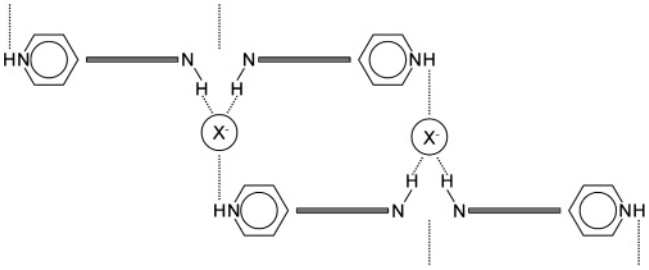

Figure 12. Pictorial sketch of a side view for the proposed hydrogen bonding model for the J-aggregation of $\{(H_6TpyP(4)^{6+})(X^-)_6\}$ ion pairs through the intermediacy of halide anions (charges and saddling distortion have been omitted for clarity; N−H bonds belong to opposite pyrrole rings).

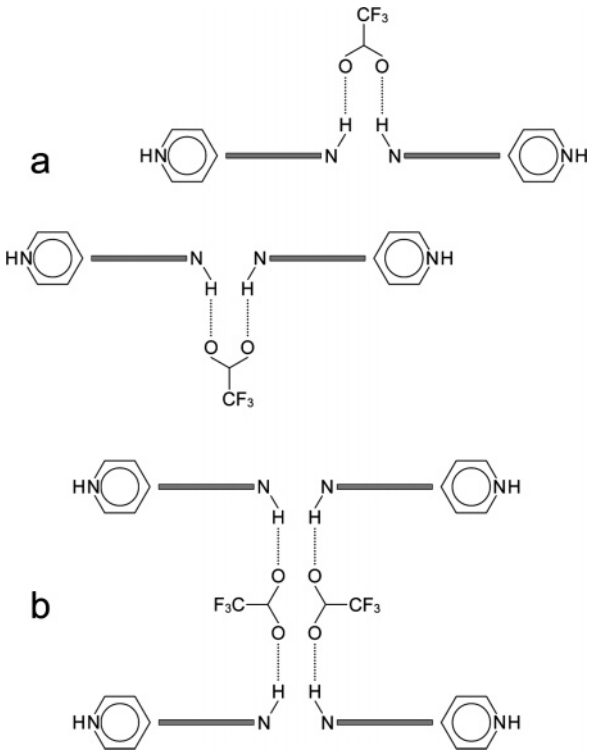

Figure 13. Pictorial sketch of side views of proposed structural models for aggregation of $\{(H_5TpyP(4)^{5+})(CF_3COO^-)_5\}$ ion pairs (lateral counteranions, charges, and saddling distortion have been omitted for clarity; N−H bonds belong to opposite pyrrole rings).

ferent kinds of structural arrangements, involving such counteranions as bridging ligands,[28] can be hypothesized for explaining the formation of aggregated species (Figure 13). In all cases, the anion plays a role in establishing a hydrogen bonding network and contributing to charge neutralization. On the basis of the observation of fairly intense and narrow RLS signals, we are inclined to think that the dimer reported in Figure 13b could be a more reasonable guess. Indeed, this structure can be easily stabilized through π-stacking interactions between adjacent dimeric units, allowing for a better electronic coupling in the resulting extended aggregate. Further addition of acid on these aggregated species (type ii behavior) leads to the diacids with coordination of a second anion on the available face of the porphyrin plane and consequent disruption of the aggregate.

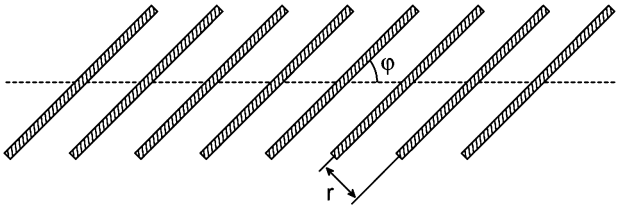

Figure 14. Schematic representation of exciton coupled J-aggregates.

An interesting feature of the obtained J-aggregates is that their spectroscopic properties are also dependent on the nature of the counteranion. This observation is not unprecedented. Indeed, a recent literature report indicates that the water-soluble porphyrin tetrakis(4-carboxyphenyl)porphyrin (TCPP) aggregates in acid media leading to species exhibiting exciton splitting which is dependent on the nature of the anion (Cl^- and NO_3^-).[29] The possibility of tuning the optical properties of J-aggregated porphyrins is considered an important key to modeling the photophysical processes in photosynthetic light-harvesting systems and for potential applications in material sciences. The exciton theory developed by Kasha[10] predicts that for interacting chromophores the dipole−dipole interaction energy V is given by

$$V = -\frac{M^2}{r^3}(1 - 3\cos^2\theta)$$

where M is the transition moment, r is the distance between the centers of the two dipoles, and θ is a geometric factor accounting for the mutual orientation of the aligned monomers. In the case of J-type aggregates, the dipole moments are parallel assuming an angle φ ($0 \leq \varphi < \pi/2$) with respect to the line connecting the centers of the dipoles (Figure 14).

As discussed in the previous section, different anions exhibit different extents of interaction with the central protonated core, affecting the energy of both the B- and Q-bands. Consequently, in the formation of the J-aggregates, the anions can influence the values of the transition moment. At the same time, they can exert an influence on the main geometric factors r and φ, acting on the packing between adjacent porphyrins. All these factors will contribute to a wide modulation of the spectral features of the final aggregates.

A further point worth noting is the possibility of exerting kinetic control over the aggregation process by simply controlling the rate of acid addition into the system. We consider the system TpyP(4) with HCl as an example of this effect. Figure 5 shows that the slow and stepwise addition of acid to the porphyrin solution produces a series of smooth spectral changes, without the clear identification of isosbestic points. By stopping the acid addition at an intermediate level, $\{(H_4TpyP(4)^{4+})(Cl^-)_4\}$ ion pair is formed and it starts to aggregate, leading to the RLS spectra shown in Figure 6b (dashed line). This species has been identified as a solid deposit on the quartz window of the cell

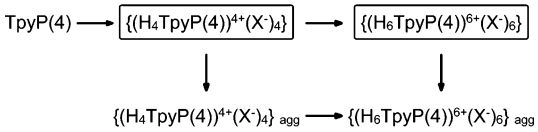

Figure 15. Possible alternative routes to protonation and aggregation for TpyP(4) with halide anions. For the sake of simplicity, explicit addition of HX in each step has been omitted.

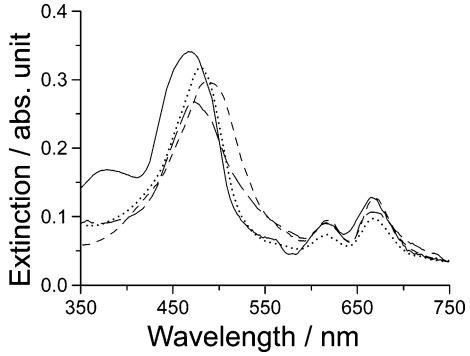

Figure 16. Comparison of UV/vis spectra of $\{(H_6TpyP(4)^{6+})(X^-)_6\}_{agg}$ aggregated species: X = Cl (solid line), Br (dashed line), mixed 4Cl/2Br (dotted line), and mixed 4Br/2Cl (long dashed line) (see text).

during the UV photoinduced generation of HCl by decomposition of dichloromethane.[19] Faster addition of acid to the initial solution does not allow the intermediate ion pair to aggregate, but drives the system to the fully protonated species $\{(H_6TpyP(4)^{6+})(Cl^-)_6\}$, which eventually aggregates (Figure 15). These observations prompted us to verify the possibility of further controlling the nature of the aggregated porphyrins. Figure 16 reports a comparison of the UV/vis extinction spectra of fully aggregated $\{(H_6TpyP(4)^{6+})(X^-)_6\}$ ion pairs obtained with HCl and HBr (Soret bands at 470 and 492 nm, respectively). Additions of HBr to preformed $\{(H_4TpyP(4)^{4+})(Cl^-)_4\}_{agg}$ and of HCl to preformed $\{(H_4TpyP(4)^{4+})(Br^-)_4\}_{agg}$ lead to new mixed species $\{(H_6TpyP(4)^{6+})(Cl^-)_4(Br^-)_2\}_{agg}$ and $\{(H_6TpyP(4)^{6+})(Br^-)_4(Cl^-)_2\}_{agg}$ having well distinct spectral features (Soret bands at 480 and 474 nm, respectively).

The hierarchical self-assembling of monomers into supramolecular structures is usually exploited in nature.[30] Many examples have been reported in the literature,[31] and quite recently a noncovalent approach based on pH-dependent equilibria involving a phosphorylated porphyrin has been demonstrated.[32]

Concluding Remarks

We have investigated the interaction of a series of isomeric protonated porphyrins with a variety of counteranions, exploiting a combination of UV/vis absorption, fluorescence emission, and RLS techniques. Our experimental findings point to a strong modulation of the protonation behavior (in terms of intermediate acidic species) and of the self-aggregation by the nature of the counteranions. At least three different patterns of behavior can be recognized as a function of the size and electronic characteristics of the anion. Most of the observed aggregated species exhibit spectroscopic features typical of J-aggregates and are interpretable on the basis of exciton coupling theory. The anions play an important role in stabilizing the aggregated structure through an interplay of hydrogen bonding, electrostatics, and dispersive forces. For these reasons, they influence the main structural and electronic parameters affecting the spectral properties of these systems, which can be predicted by theoretical methods (TDDFT).[17] The hierarchy of the aggregation process offers the possibility of fine-tuning the important optical features of such species, by simply changing the counteranion or controlling the rate of acid addition, and opens the way to exploiting these aggregates in the material sciences and in nanotechnology.

Acknowledgment. The authors thank the MIUR, PRIN-COFIN 2004, for financial support.

References and Notes

(1) White, W. I. In *The Porphyrins*; Dolphin, D., Ed.; Academic Press: New York, 1978; Vol. 5, p 303.
(2) Pullerits, T.; Sundstrom, V. *Acc. Chem. Res.* **1996**, *29*, 381−389.
(3) Schenning, A.; Benneker, F. B. G.; Geurts, H. P. M.; Liu, X. Y.; Nolte, R. J. M. *J. Am. Chem. Soc.* **1996**, *118*, 8549−8552. Hofkens, J.; Latterini, L.; Vanoppen, P.; Faes, H.; Jeuris, K.; DeFeyter, S.; Kerimo, J.; Barbara, P. F.; DeSchryver, F. C.; Rowan, A. E.; Nolte, R. J. M. *J. Phys. Chem. B* **1997**, *101*, 10588−10598.
(4) Balaban, T. S.; Bhise, A. D.; Fischer, M.; Linke-Schaetzel, M.; Roussel, C.; Vanthuyne, N. *Angew. Chem., Int. Ed.* **2003**, *42*, 2140−2144.
(5) Drain, C. M.; Batteas, J. D.; Flynn, G. W.; Milic, T.; Chi, N.; Yablon, D. G.; Sommers, H. *Proc. Natl. Acad. Sci. U.S.A.* **2002**, *99*, 6498−6502.
(6) Castriciano, M.; Romeo, A.; Villari, V.; Micali, N.; Scolaro, L. M. *J. Phys. Chem. B* **2004**, *108*, 9054−9059.
(7) Pasternack, R. F.; Goldsmith, J. I.; Szep, S.; Gibbs, E. J. *Biophys. J.* **1998**, *75*, 1024−1031. Kano, K.; Minamizono, H.; Kitae, T.; Negi, S. *J. Phys. Chem. A* **1997**, *101*, 6118−6124.
(8) Pancoska, P.; Urbanova, M.; Bednarova, L.; Vacek, K.; Paschenko, V. Z.; Vasiliev, S.; Malon, P.; Kral, M. *Chem. Phys.* **1990**, *147*, 401−413. Pasternack, R. F.; Gibbs, E. J. *J. Inorg. Organomet. P.* **1993**, *3*, 77−88. Nezu, T.; Ikeda, S. *Bull. Chem. Soc. Jpn.* **1993**, *66*, 25−31. Purrello, R.; Scolaro, L. M.; Bellacchio, E.; Gurrieri, S.; Romeo, A. *Inorg. Chem.* **1998**, *37*, 3647−3648. Purrello, R.; Bellacchio, E.; Gurrieri, S.; Lauceri, R.; Raudino, A.; Scolaro, L. M.; Santoro, A. M. *J. Phys. Chem. B* **1998**, *102*, 8852−8857. Bellacchio, E.; Lauceri, R.; Gurrieri, S.; Scolaro, L. M.; Romeo, A.; Purrello, R. *J. Am. Chem. Soc.* **1998**, *120*, 12353−12354. Purrello, R.; Raudino, A.; Scolaro, L. M.; Loisi, A.; Bellacchio, E.; Lauceri, R. *J. Phys. Chem. B* **2000**, *104*, 10900−10908.
(9) Castriciano, M. A.; Romeo, A.; Scolaro, L. M. *J. Porphyrins Phthalocyanines* **2002**, *6*, 431−438.
(10) McRae, E. G.; Kasha, M. *J. Chem. Phys.* **1958**, *28*, 721−722. McRae, E. G.; Kasha, M. In *Physical Processes in Radiation Biology*; Augenstein, L., Mason, R., Rosenberg, B., Eds.; Academic Press: New York, 1964; pp 23−42.
(11) Knapp, E. W. *Chem. Phys.* **1984**, *85*, 73−82.
(12) Ohno, O.; Kaizu, Y.; Kobayashi, H. *J. Chem. Phys.* **1993**, *99*, 4128−4139. Ribo, J. M.; Crusats, J.; Farrera, J. A.; Valero, M. L. *J. Chem. Soc., Chem. Commun.* **1994**, 681−682. Ribo, J. M.; Rubires, R.; El-Hachemi, Z.; Farrera, J. A.; Campos, L.; Pakhomov, G. L.; Vendrell, M. *Mater. Sci. Eng. C: Biomimetic Supramol. Syst.* **2000**, *11*, 107−115. Akins, D. L.; Zhu, H. R.; Guo, C. *J. Phys. Chem.* **1994**, *98*, 3612−3618. Akins, D. L.; Ozcelik, S.; Zhu, H. R.; Guo, C. *J. Phys. Chem.* **1996**, *100*, 14390−14396. Maiti, N. C.; Ravikanth, M.; Mazumdar, S.; Periasamy, N. *J. Phys. Chem.* **1995**, *99*, 17192−17197. Koti, A. S. R.; Taneja, J.; Periasamy, N. *Chem. Phys. Lett.* **2003**, *375*, 171−176. Schwab, A. D.; Smith, D. E.; Rich, C. S.; Young, E. R.; Smith, W. F.; de Paula, J. C. *J. Phys. Chem. B* **2003**, *107*, 11339−11345. Rotomskis, R.; Augulis, R.; Snitka, V.; Valiokas, R.; Liedberg, B. *J. Phys. Chem. B* **2004**, *108*, 2833−2838.
(13) Castriciano, M.; Romeo, A.; Villari, V.; Micali, N.; Scolaro, L. M. *J. Phys. Chem. B* **2003**, *107*, 8765−8771. Micali, N.; Mallamace, F.; Romeo, A.; Purrello, R.; Scolaro, L. M. *J. Phys. Chem. B* **2000**, *104*, 5897−5904.
(14) Pasternack, R. F.; Schaefer, K. F.; Hambright, P. *Inorg. Chem.* **1994**, *33*, 2062−2065.
(15) Akins, D. L.; Zhu, H. R.; Guo, C. *J. Phys. Chem.* **1996**, *100*, 5420−5425.
(16) Stone, A.; Fleischer, E. B. *J. Am. Chem. Soc.* **1968**, *90*, 2735−2748.
(17) Rosa, A.; Ricciardi, G.; Baerends, E. J.; Romeo, A.; Scolaro, L. M. *J. Phys. Chem. A* **2003**, *107*, 11468−11482.
(18) Khairutdinov, R. F.; Serpone, N. *J. Phys. Chem. B* **1999**, *103*, 761−769.
(19) Scolaro, L. M.; Romeo, A.; Castriciano, M. A.; De Luca, G.; Patane, S.; Micali, N. *J. Am. Chem. Soc.* **2003**, *125*, 2040−2041.
(20) Kalyanasundaram, K. *Inorg. Chem.* **1984**, *23*, 2453−2459.
(21) Brookhart, M.; Grant, B.; Volpe, A. F. *Organometallics* **1992**, *11*, 3920−3922.
(22) Pasternack, R. F.; Collings, P. J. *Science* **1995**, *269*, 935−939.
(23) Strauss, S. H. *Chem. Rev.* **1993**, *93*, 927−942.
(24) Aronoff, S. *J. Phys. Chem.* **1958**, *62*, 428−431.
(25) Rau, W. G.; Longo, F. R. *Inorg. Chem.* **1977**, *16*, 1372−1376.

(26) Parkash, J.; Robblee, J. H.; Agnew, J.; Gibbs, E.; Collings, P.; Pasternack, R. F.; de Paula, J. C. *Biophys. J.* **1998**, *74*, 2089−2099.

(27) Kano, K.; Fukuda, K.; Wakami, H.; Nishiyabu, R.; Pasternack, R. F. *J. Am. Chem. Soc.* **2000**, *122*, 7494−7502. Barber, D. C.; Freitag-Beeston, R. A.; Whitten, D. G. *J. Phys. Chem.* **1991**, *95*, 4074−4086.

(28) TDDFT calculations predict that a monodentate binding mode for the CF_3COO^- anion should easily lead to hydrogen removal from the monoacid species. This observation supports the hypothesis of a bridging binding mode for the carboxylate ligand. Ricciardi, G.; Rosa, A. Private communication.

(29) Choi, M. Y.; Pollard, J. A.; Webb, M. A.; McHale, J. L. *J. Am. Chem. Soc.* **2003**, *125*, 810−820.

(30) Lehn, J. M. *Supramolecular Chemistry*; VCH: Weinheim, 1995.

(31) Prins, L. J.; Timmerman, P.; Reinhoudt, D. N. *J. Am. Chem. Soc.* **2001**, *123*, 10153−10163. Petitjean, A.; Cuccia, L. A.; Lehn, J. M.; Nierengarten, H.; Schmutz, M. *Angew. Chem., Int. Ed.* **2002**, *41*, 1195−1198. Wong, G. C. L.; Tang, J. X.; Lin, A.; Li, Y. L.; Janmey, P. A.; Safinya, C. R. *Science* **2000**, *288*, 2035−2039. Velonia, K.; Rowan, A. E.; Nolte, R. J. M. *J. Am. Chem. Soc.* **2002**, *124*, 4224−4225. Brunsveld, L.; Vekemans, J.; Hirschberg, J.; Sijbesma, R. P.; Meijer, E. W. *Proc. Natl. Acad. Sci. U.S.A.* **2002**, *99*, 4977−4982.

(32) De Napoli, M.; Nardis, S.; Paolesse, R.; Vicente, M. G. H.; Lauceri, R.; Purrello, R. *J. Am. Chem. Soc.* **2004**, *126*, 5934−5935.